How to cite: *Angew. Chem. Int. Ed.* **2021**, *60*, 18666–18672
International Edition: doi.org/10.1002/anie.202104461
German Edition: doi.org/10.1002/ange.202104461

Metal–Organic Frameworks | Hot Paper

Surface-Modified Phthalocyanine-Based Two-Dimensional Conjugated Metal–Organic Framework Films for Polarity-Selective Chemiresistive Sensing

Mingchao Wang[+], Zhe Zhang[+], Haixia Zhong, Xing Huang, Wei Li, Mike Hambsch, Panpan Zhang, Zhiyong Wang, Petko St. Petkov, Thomas Heine, Stefan C. B. Mannsfeld, Xinliang Feng,* and Renhao Dong**

Abstract: *2D conjugated metal–organic frameworks (2D c-MOFs) are emerging as electroactive materials for chemiresistive sensors, but selective sensing with fast response/recovery is a challenge. Phthalocyanine-based $Ni_2[MPc(NH)_8]$ 2D c-MOF films are presented as active layers for polarity-selective chemiresisitors toward water and volatile organic compounds (VOCs). Surface-hydrophobic modification by grafting aliphatic alkyl chains on 2D c-MOF films decreases diffused analytes into the MOF backbone, resulting in a considerably accelerated recovery progress (from ca. 50 to ca. 10 s) during humidity sensing. Toward VOCs, the sensors deliver a polarity-selective response among alcohols but no signal for low-polarity aprotic hydrocarbons. The octadecyltrimethoxysilane-modified $Ni_2[MPc(NH)_8]$ based sensor displays high-performance methanol sensing with fast response (36 s)/recovery (13 s) and a detection limit as low as 10 ppm, surpassing reported room-temperature chemiresistors.*

Introduction

Two-dimensional conjugated metal–organic frameworks (2D *c*-MOFs),[1] which are van der Waals layer-stacked MOFs with high in-plane π-d conjugation,[2] have emerged as new-generation electroactive materials for multifunctional devices, such as field-effect transistors,[3] photodetectors,[4] thermoelectrics,[5] spintronics,[6] superconductors,[7] and energy storage[8] and conversion.[9] Particularly, 2D *c*-MOFs have been demonstrated to exhibit high performance for chemiresistive sensors due to their abundant active sites and intrinsic conductivity.[10] For instance, chemiresistors based on $Cu_3(HHTP)_2$[11] (HHTP = 2,3,6,7,10,11-hexaoxytriphenylene[12]) and $M_3(HITP)_2$ (HITP = 2,3,6,7,10,11-hexaiminotriphenylene, M = Cu or Ni)[13] were capable of detecting ammonia and volatile organic compounds (VOCs) at the parts per million (ppm) level. In addition, linking phthalocyanine (Pc) units with square-planar metal complex endows the resultant 2D *c*-MOF with additional active sites due to potential intermolecular interactions between Pc and analytes.[14] The reported chemiresistors via drop-casting Pc-based 2D *c*-MOF powder samples have exhibited effective sensing toward NH_3, H_2S, and NO with the response/recovery in the order of minutes,[15] which represents the state-of-art performance for these analytes among 2D *c*-MOF based chemiresistors.[10,11,13b,16]

Despite the preliminary success, the sensors integrated via mechanical compression or drop-casting of the 2D *c*-MOF powders, were often associated with sacrificed pore volume and suppressed charge transport,[17] thus resulting in sluggish response and recovery as well as poor detection limit. To address the above challenges, 2D *c*-MOF thin films have been recently developed via wet-interface-assisted gas-liquid,[1c,18] liquid-liquid,[7,19] and liquid-solid[20] approaches, allowing long-range charge transport and facile circuit integration with good contacts.[20a,b,21] Nevertheless, a fast recovery after the detection has not been realized (the reported recovery times were generally longer than 2 min),[11,13,15,20a] due to the lack of synthetic control over the morphology, thickness, and the surface property (e.g., functional groups) of MOF film that

[*] M. Wang,[+] Z. Zhang,[+] Dr. H. Zhong, Dr. X. Huang, Dr. W. Li, Dr. P. Zhang, Z. Wang, Prof. T. Heine, Prof. X. Feng, Dr. R. Dong
Center for Advancing Electronics Dresden (cfaed) and Faculty of Chemistry and Food Chemistry, Technische Universität Dresden
01062 Dresden (Germany)
E-mail: xinliang.feng@tu-dresden.de
Renhao.dong@tu-dresden.de

Z. Zhang,[+] Dr. M. Hambsch, Prof. S. C. B. Mannsfeld
Center for Advancing Electronics Dresden (cfaed) and Faculty of Electrical and Computer Engineering
Technische Universität Dresden
01062 Dresden (Germany)
E-mail: stefan.mannsfeld@tu-dresden.de

Dr. P. St. Petkov
Faculty of Chemistry and Pharmacy, University of Sofia
1164 Sofia (Bulgaria)

Prof. T. Heine
Helmholtz-Zentrum Dresden-Rossendorf
Institute of Resource Ecology, Leipzig Research Branch
04316 Leipzig (Germany)

[+] These authors contributed equally to this work.

Supporting information and the ORCID identification number(s) for the author(s) of this article can be found under: https://doi.org/10.1002/anie.202104461.

plays an important role to the interaction of analyte and MOF. In addition, the low selectivity has remained another challenge for MOF-based sensors.[22] Surface-modification has been widely employed to modify the surface wettability of 2D materials (such as graphene and graphene oxide)[10,23] and three-dimensional MOF[24] for sensing, thus improving the sensitivity, selectivity and recovery speed. However, related modification on 2D *c*-MOFs with the aim of improving the sensing performance remains unexplored.

Herein, we synthesize polycrystalline Pc-based nickel-bis(diimine) ($Ni(NH)_4$)-linked 2D *c*-MOF thin films ($Ni_2[MPc(NH)_8]$, M = Cu or Ni) with large area (several cm^2) and tunable thickness (70 to ca. 500 nm) at a liquid (dimethyl sulfoxide, DMSO)/solid (SiO_2) interface. The resultant films exhibited high electrical conductivity (0.3–0.6 S cm) and intrinsic porous structure with square lattice. Then, we demonstrate the first example of surface-modification on 2D *c*-MOFs by various surface functional groups, thus enabling the surface wettability tailored from hydrophilic to hydrophobic. Grafting alkylamine on $Ni_2[MPc(NH)_8]$ (with minor change of surface wettability) has a negligible effect on the humidity sensing. However, grafted hydrophobic aliphatic alkyl chains reduce the diffusing amount of water molecules into the MOF backbone, hence significantly improving the recovery progress (time of ca. 10 s, 600 ppm H_2O) compared with the pristine film sample (ca. 50 s). This modification strategy by aliphatic alkyl chains also works for methanol sensing, evidenced by improved response and recovery performance of 36 and 13 s, respectively (recovery of > 50 s for the original sample). Remarkably, the modified 2D *c*-MOF based sensors are capable of methanol-sensing at a 10 ppm level which surpasses the state-of-art reported chemiresistors at room-temperature based on MOFs, conducting polymers, black phosphorus, Mxenes, metal disulfides, and most of the metal oxides (Supporting Information, Tables S1,S2). Notably, the resultant sensors deliver a polarity-selective response toward VOCs. For instance, methanol molecules, which have higher polarity and higher dielectric constant than other alcohol molecules, can be detected the most efficiently among alcohols, due to their strongest affinity to the $Ni(NH)_4$-linkage of $Ni_2[MPc(NH)_8]$. Our work highlights surface modification of semiconducting 2D *c*-MOF films toward polarity-selective chemiresistive sensing with fast response/recovery and low detection limit, thus further pushing the development of conductive MOFs for applications in electronics.

Results and Discussion

Large-area (cm^2) $Ni_2[MPc(NH)_8]$ (M = Cu or Ni) 2D *c*-MOF films (Figure 1a) were synthesized at a liquid-solid interface by placing a SiO_2/Si substrate in the solution of metal (II) 2,3,9,10,16,17,23,24-octaaminophthalocyanine, $Ni(NO_3)_2$, $NH_3{\cdot}H_2O$ and DMSO in air (see details in the Supporting Information). Field-emission scanning electron

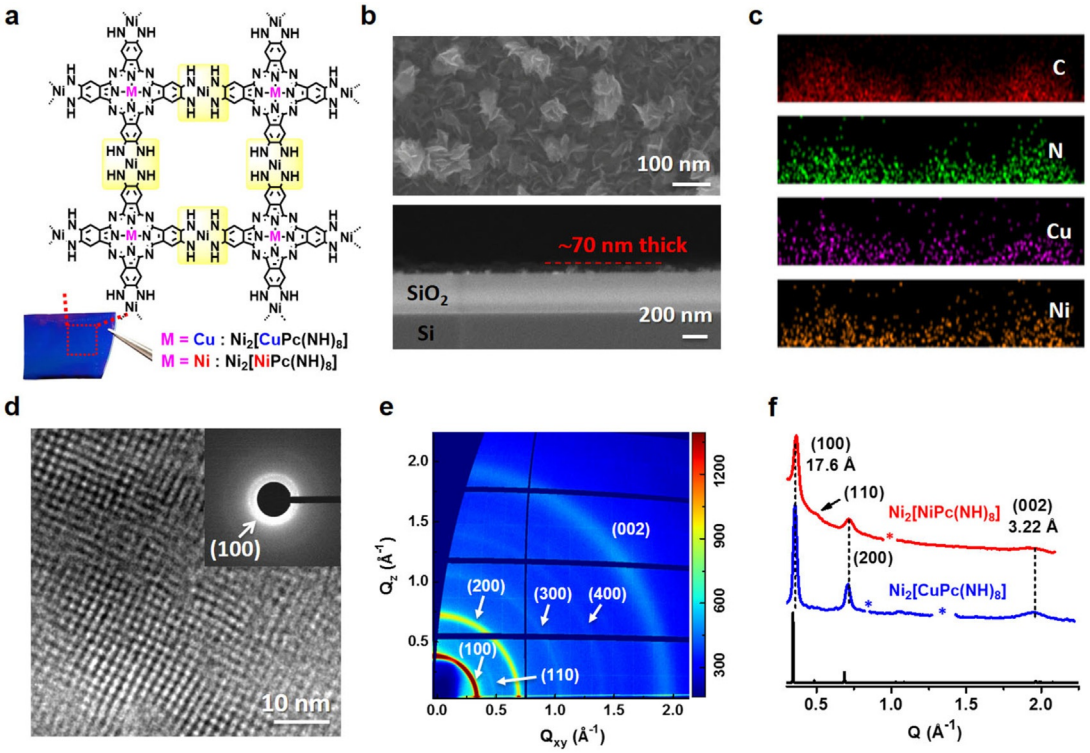

Figure 1. $Ni_2[MPc(NH)_8]$ 2D *c*-MOF films (M = Cu or Ni). a) Chemical structure and the optical image of the as-synthesized film (ca. 70 nm thick) on SiO_2/Si wafer. The $Ni(NH)_4$-linkage of $Ni_2[MPc(NH)_8]$ 2D *c*-MOF is highlighted yellow. b),c) Top- and side-view SEM images and side-view EDX images of $Ni_2[CuPc(NH)_8]$ film. d) HR-TEM image of $Ni_2[CuPc(NH)_8]$. The inset is the SAED pattern. e) GIWAXS pattern of the $Ni_2[CuPc(NH)_8]$ film. f) X-ray diffraction (XRD) patterns derived from the GIWAXS data of $Ni_2[CuPc(NH)_8]$ (blue) and $Ni_2[NiPc(NH)_8]$ (red) as well as the simulated XRD pattern referring to the AA-serrated stacking (black).[8b]

microscopy (FE-SEM) images indicate that the films are composed of continuously aggregated sheet-like crystallites, and the thickness of the films could be tuned from ca. 500 to ca. 70 nm by increasing reaction temperature from 50 to 60 °C (Figure 1b and Figures S1,S2). Energy-dispersive X-ray (EDX) and X-ray photoelectron spectroscopy (XPS) measurements reveal a homogeneous distribution of C, N, and metal elements throughout the film (Figure 1c and Figures S3–S6). High-resolution transmission electron microscopy (HR-TEM) and selected-area electron diffraction (SAED) measurements resolve crystalline 2D *c*-MOF with square unit cells of $a = b \approx 1.7$ nm (Figure 1d). Grazing incidence wide angle X-ray scattering (GIWAXS) pattern suggests ordered structure with intensive peaks at 0.35, 0.71, and 1.95 $Å^{-1}$ for both $Ni_2[CuPc(NH)_8]$ and $Ni_2[NiPc(NH)_8]$ samples (Figure 1e and Figure S7). Compared with the calculated diffraction pattern, we assigned the observed peaks to (100), (200), and (002) lattice planes, respectively, which correspond to a AA-serrated stacking model (Figure 1f).[8b] To modulate the surface property of the as-synthesized MOF films, we performed the surface-modification by the modification with various insulating silanes, which comprise different functional groups (e.g., alkylamine, aromatic or aliphatic hydrocarbon, termed as (3-aminopropyl)trimethoxysilane (APTMS), phenyltrichlorosilane (PTCS) and octadecyltrimethoxysilane (OTMS) in Figure 2a and Figure S8). The solutions of silanes were spin-coated on $Ni_2[MPc(NH)_8]$ film surface, followed by ammonia treatment (details are shown in Supporting Information). To understand the interaction between silane and 2D *c*-MOFs, we selected OTMS-modified $Ni_2[MPc(NH)_8]$ (named as $Ni_2[MPc(NH)_8]$-OTMS, M = Cu or Ni) as typical examples (Figure S9). Fourier-transform infrared (FTIR) spectra reveal the presence of aliphatic C–H stretching (CH_2: 2842, 2911 cm^{-1} and CH_3: 2957 cm^{-1}) vibrational bands (Figure 2b and Figure S10), that suggests the successful modification by OTMS. XRD patterns indicate that the crystal structures and the interlayer distances of $Ni_2[MPc(NH)_8]$ retain, while an additional peak with 2θ at 21.4° is assignable to the crystallized OTMS (Figure 2c and Figure S11).[25] The porosity of $Ni_2[CuPc(NH)_8]$-OTMS was investigated by the N_2 adsorption/desorption, which reveals that the presence of self-assembled OTMS in this modified sample leads to a slightly declined surface-area in contrast to pristine $Ni_2[CuPc(NH)_8]$ (Figure S12). The pore size distribution via density functional theory method shows a retained pore size as ca. 12.3 Å after the OTMS-modification (Figure S12, inset), excluding potential penetration of OTMS into the $Ni_2[CuPc(NH)_8]$ backbone. Next, we synthesized Ni-$(NH)_4$-linkage (named as $Ni[C_6H_4(NH)_2]_2$) and Pc building block (named as $^tBu_4NiPc$) as model compounds to understand the above silane-modification (structures are shown in Figures 4c,d). ^1H nuclear magnetic resonance (NMR) spectra indicate no structural change for both $Ni(NH)_4$ and the Pc units after OTMS-treatment, which reveals the absence of chemical bond formation between 2D *c*-MOF and OTMS (Figures S13–S15). Based on the above multiple analysis we confirmed that the crystalline silane layer adsorbed physically on the macroscopic 2D *c*-MOF films. To evaluate the surface wettability of these films, water contact angle (WCA) measurements were conducted before and after surface-modification. For instance, pristine $Ni_2[CuPc(NH)_8]$ was hydrophilic with WCA value of ca. 55° (Figure 2d), due to the presence of abundant hydrophilic imine groups in the $Ni(NH)_4$ linkages (Figures S16,S17). The WCA value was increased to 85° after APTMS-modification, and further increased to 113° after grafting benzene ring (PTCS). Upon grafting the aliphatic alkyl chains (OTMS), the surface became highly hydrophobic with WCA of 138°.

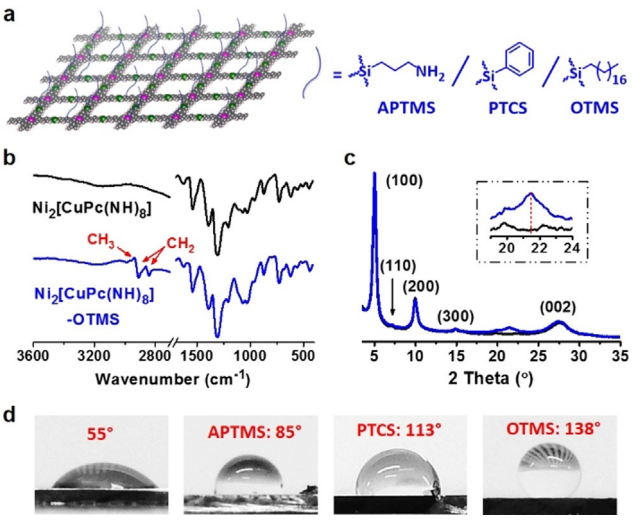

Figure 2. a) Illustration of the surface-modification of $Ni_2[CuPc(NH)_8]$ 2D *c*-MOF film with APTMS, PTCS, and OTMS. b) FTIR spectra of $Ni_2[CuPc(NH)_8]$ (black) and $Ni_2[CuPc(NH)_8]$-OTMS (blue). c) XRD patterns of pristine $Ni_2[CuPc(NH)_8]$ (black) and $Ni_2[CuPc(NH)_8]$-OTMS (blue). The insets are the enlarged patterns at around 22°. d) Water contact angle measurements of pristine $Ni_2[CuPc(NH)_8]$ (WCA = 55°) and the surface-modified films.

The surface potential of the $Ni_2[CuPc(NH)_8]$ films was estimated by Kelvin probe force microscopy (KPFM), which revealed that the pristine film possessed a work function of 0.30 eV and the surface-modification showed a negligible effect on the work function (Figures S18,S19). Subsequently, the electrical conductivity was measured via 2-probe method at ambient conditions. The linear current–voltage curves confirm an ohmic contact (Figure S20a) and provide a conductivity of ca. 0.6 S cm for $Ni_2[CuPc(NH)_8]$ (ca. 0.3 S cm for $Ni_2[NiPc(NH)_8]$, Table S3). Variable-temperature (*T*) conductivity measurement of $Ni_2[CuPc(NH)_8]$ in the van der Pauw configuration indicated a drop of conductivity upon cooling and suggested a conductivity of ca. 0.7 S cm at 300 K (Figure S20b,c). The plot of conductivity versus $T^{-1/4}$ can be well fitted to the Mott-law variable range hopping model (Figure S20c, inset), which illustrates a hopping conductivity in this polycrystalline film sample. After surface-modification by various silanes, the MOF film showed declined conductivity with the values of 0.2–0.4 S cm (2-probe, Table S4).

Next, pristine $Ni_2[CuPc(NH)_8]$ film on SiO_2/Si (ca. 70 nm) was integrated into a chemiresistive device by depositing gold electrodes with channel length of 100 μm between the gold electrodes (Figure 3a). Upon an exposure to 600 ppm H_2O, a sharp decrease in current was recorded within seconds (Figure S21). After 120 s, a response intensity (response =-

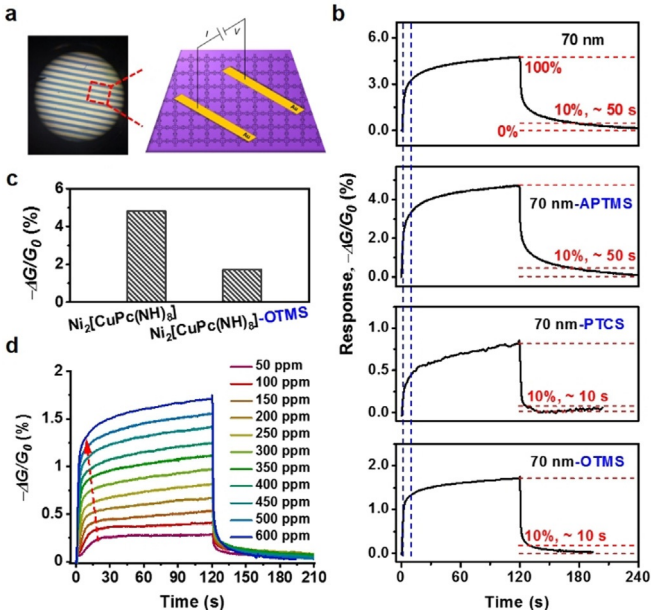

Figure 3. a) Microscope image and illustration of the fabricated chemiresistor device. b) Humidity sensing of $Ni_2[CuPc(NH)_8]$ film before and after surface-modification under 600 ppm H_2O. The response curves from top to bottom refer to pristine, APTMS-, PTCS-, and OTMS-modified films (ca. 70 nm thick), respectively. c) $-\Delta G/G_0$ values of pristine and OTMS-modified $Ni_2[CuPc(NH)_8]$ to 600 ppm H_2O. d) Concentration-dependent response curves of $Ni_2[CuPc(NH)_8]$-OTMS to H_2O vapor.

$\Delta G/G_0 = -(I-I_0)/I_0 \times 100\,\%$, I is current whilst I_0 represents the initial current) was calculated as 4.7 % (Figure 3 b, top). As contrast, the sensors based on the ca. 500 nm-thick film and the pelletized bulk sample (ca. 0.3 mm-thick) displayed much inferior humidity sensing with $-\Delta G/G_0 < 0.3\,\%$ (Figures S22). This can be attributed to the numerous grain boundaries[20a] or randomly orientated crystallites in the thick samples[1d] that slow the gas diffusion and hamper the charge transport in these samples, thus resulting in slow signal-transduction. The above contrast experiments suggest that highly crystalline MOF thin films are critical for a high-performance sensing device.

We then investigated the influence of surface modification on the sensing performance. Grafting alkylamine (APTMS) on the 70 nm-thick $Ni_2[CuPc(NH)_8]$ film showed a negligible effect on the response/recovery under the above experimental conditions (Figure 3 b). On the contrary, lower $-\Delta G/G_0$ value for $Ni_2[CuPc(NH)_8]$-OTMS sample was determined as 1.7 % (@ 120 s) compared with the pristine sample (Figure 3 c); the response rate remained almost unaffected, while the recovery was significantly accelerated from ca. 50 to ca. 10 s (Figure 3 b, bottom and Figure S23). The hydrophobic alkyl chains on $Ni_2[CuPc(NH)_8]$ reduced the amount of diffused H_2O molecules into the 2D *c*-MOF backbone during the same exposure time, thus inducing an easier and faster elimination of the adsorbed H_2O molecules in the recovery step. The resolved fast recovery within ca. 10 s at such a low humidity level (600 ppm = 3.8 % relative humidity (RH)) is superior to the thus-far reported room-temperature humidity chemiresistors based on MOFs,[10,26] covalent organic frameworks,[27] and conducting polymers,[28] and even comparable to graphene oxide,[29] metal oxides,[30] metal disulfides[31] at high humidity level of 43–100 % RH (details seen in Table S5). As the water concentration decreased from 600 to 50 ppm (ca. 0.3 % RH), a reproducible concentration-dependent-response was recorded (Figure 3 d). By contrast, the PTCS- modified samples exhibited inferior performance with slow response (Figure 3 b). In addition, the OTMS-modification on the isostructural $Ni_2[NiPc(NH)_8]$ film resulted in similar surface hydrophobic behavior (Figure S24) and an enhancement in the recovery process in humidity sensing as well (Figure S25). However, $Ni_2[NiPc(NH)_8]$-OTMS displayed inferior performance compared with $Ni_2[CuPc(NH)_8]$-OTMS, that could be ascribed to the lower conductivity of the former thus resulting in relatively sluggish signal-transduction.

We also investigated the chemiresistive sensing toward methanol, a typical VOC with human toxicity,[10] before and after OTMS-surface-modification (Figure S26). Toward 400 ppm methanol, the $Ni_2[CuPc(NH)_8]$-OTMS based sensor displayed significantly faster response/recovery process (Figure 4 a) than those based on the pristine sample (Figure S27). Further extending the exposure time from 120 to 600 s results in no obvious change (Figure S28). Based on an equilibrium response of $Ni_2[CuPc(NH)_8]$-OTMS, a response time (90 % of the saturation value[10]) and a recovery time (10 % of the saturation value[10]) were obtained as 36 and 13 s, respectively (Figure S28b), which surpass the thus-far reported 2D *c*-MOFs and traditional MOFs for chemiresistive methanol sensing at room temperature (Table S1).[13a,32] As the methanol concentration decreased to 10 ppm, $-\Delta G/G_0$ decreased to 0.23 % (3.22 % at 400 ppm) and the characteristic times increased (Figure 4 a). To be noted, the device retained its

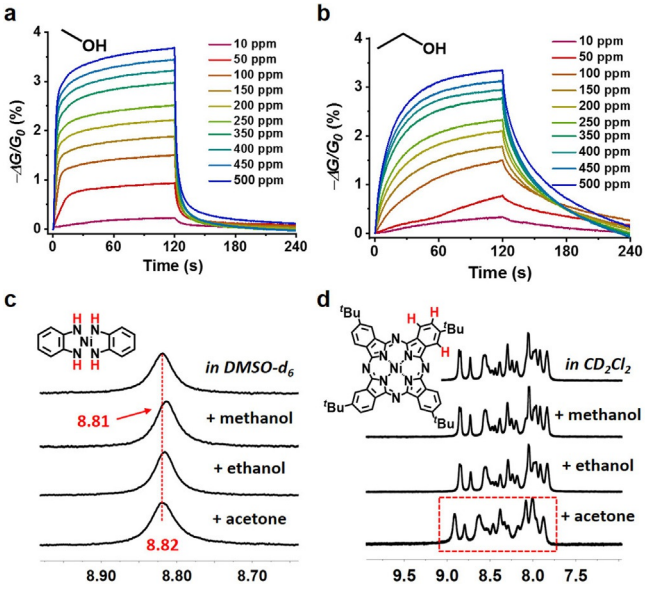

Figure 4. a),b) Response curves of $Ni_2[CuPc(NH)_8]$-OTMS toward methanol and ethanol, respectively. c) ^1H NMR spectrum of $Ni[C_6H_4(NH)_2]_2$ in $[D_6]$DMSO (top) and the spectra with the presence of 1/60 (in volume) methanol, ethanol, or acetone. d) ^1H NMR spectrum of $^tBu_4NiPc$ in CD_2CCl_2 (top) and the spectra with the presence of 1/60 (in volume) methanol, ethanol, or acetone.

high efficiency after storing at ambient conditions over one year (Figure S29), indicative of the high stability of the modified sample that holds great potential for practical application. The detection limit reached as low as 10 ppm (ca. 50 ppm for pristine sample, Figure S30), superior to the state-of-art chemiresistors at room temperature based on the other MOFs, conducting polymers, black phosphorus, Mxenes, metal disulfides, and most of the metal oxides (in the order of hundred ppm normally, Table S1,2).[13a,32,33] Notably, at high temperature (e.g., > 100 °C)[34] or upon additional modulation (e.g., application of ultraviolet light),[35] some metal oxides based chemiresistors were reported to be capable of detecting methanol in the sub-ppm level. This surface-modification strategy holds great promise in effectively improving the sensing performance of $Ni_2[MPc(NH)_8]$.

With the aim of exploring the selectivity of these sensors, we conducted sensing measurements toward VOCs with different polarity properties (polarity: methanol > ethanol > isopropanol).[36] Compared with methanol, $Ni_2[CuPc(NH)_8]$-OTMS exhibited rather slow response and recovery to 400 ppm ethanol (Figure 4b and Figure S31,S32). While for isopropanol, the sensing remained largely unsaturated after even an exposure of 600 s that failed to efficiently detect isopropanol (Figure S33). A similar sensing phenomenon was also observed for both the pristine and the OTMS-modified $Ni_2[NiPc(NH)_8]$ film (Figures S34,S35), and these results were repeatable with different batches of samples (Figure S36,S37). Given that both $Ni_2[CuPc(NH)_8]$-OTMS and $Ni_2[NiPc(NH)_8]$-OTMS were capable of distinguishing the alcohol vapors via diverse response curves (Figure S38), a polarity-dependent sensing selectivity was thus established. Methanol molecules possess higher polarity and higher dielectric constant than the other alcohols, and display stronger affinity to the linkage of $Ni_2[MPc(NH)_8]$ that was revealed by the observed shift and proton-exchange in the ^{1}H NMR spectra (Figure 4c, details seen in Figures S39–S41). Thus, methanol analyte is able to diffuse fast into the $Ni_2[MPc(NH)_8]$ porous backbone, leading to a faster response than the other alcohols. Further analysis suggested that the Pc building blocks had no interaction with above alcohols (Figure 4d and Figure S42). The different intensity of the signals ($-\Delta G/G_0$ values) could be related to their distinct dielectric constants (ε, methanol (32.70) > ethanol (24.55) > isopropanol (19.92)).[36] We note that, other common organic compounds possessing similar dielectric constant to methanol or ethanol ($\varepsilon > 24$) are non-volatile, such as dimethylformamide and DMSO.[36] Compared with the protic VOCs (alcohols), aprotic VOCs possess significantly lower dielectric constants (e.g., $\varepsilon_{acetone} = 20.70$, $\varepsilon_{chloroform} = 4.81$, $\varepsilon_{toluene} = 2.38$, $\varepsilon_{cyclohexane} = 2.02$).[36] Toward these analytes, the MOF-based devices also presented polarity-dependent sensing (polarity: acetone > chloroform > toluene > cyclohexane),[36] however, with much weaker intensity of the signals (Figure 5a and Figures S43–S46). Interestingly, though acetone molecules showed no affinity to the $Ni(NH)_4$-linkages, they interacted with the Pc building blocks, as shown in the ^{1}H NMR spectra (Figures 4c,d, bottom and Figures S47,S48). This result highlights the advantage of the Pc-based 2D *c*-MOFs that is able to immobilize bi-active-sites for selective sensing. However,

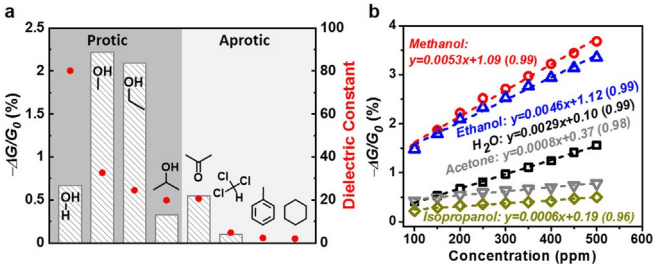

Figure 5. a) $-\Delta G/G_0$ (column) values of $Ni_2[CuPc(NH)_8]$-OTMS toward 200 ppm protic and aprotic analytes and their dielectric constants (red spot). b) Plots of $-\Delta G/G_0$ to various analytes as a function of concentrations for $Ni_2[CuPc(NH)_8]$-OTMS. The R^2 values are shown in the parentheses.

a comprehensive fundamental understanding of the sensing mechanism remains challenging, which relies on the future development of single-layer or single-crystalline 2D *c*-MOF film sample together with the application of molecule-level characterization technologies to address.

Finally, we made a further understanding about the influence of analyte molecular diffusion on the selectivity and the sensing performance. Figure 5b shows the plots of $-\Delta G/G_0$ (at 120 s) of $Ni_2[CuPc(NH)_8]$-OTMS versus concentrations (100–500 ppm), which reveals linearities ($R^2 = 0.99$) for the probed analytes, e.g., H_2O, methanol, ethanol (for $Ni_2[NiPc(NH)_8]$-OTMS seen in Figure S46). Fitting the curves provide the sensitivities (S_0, slope of the linear fitting) of $Ni_2[CuPc(NH)_8]$-OTMS based sensor, which are 0.0029, 0.0053 and 0.0046 % ppm^{-1}, respectively. We further represent the above response curves in Figure 3 and 4 with stretched exponential function:

$$-\Delta G/G_o = cS_0\left(1 - e^{-\frac{t}{\tau}}\right) \quad (1)$$

(c is concentration, t is exposure time).[37] The related fitting provided a relaxation time (τ), which corresponds to the inflexion point in the response curve at each concentration level. To be noted, τ represents no actual parameter, but an index to compare the response rate quantitatively for different analytes. As shown in Table S6, τ was estimated as 3.8, 4.0, and 18.6 s for $Ni_2[CuPc(NH)_8]$-OTMS toward 400 ppm H_2O, methanol, and ethanol, respectively. The fitting for $Ni_2[NiPc(NH)_8]$-OTMS exhibited similar values (Table S7). These results, in accordance with the above determined response times, reveal a significant contribution of the strong affinity between the polar guest molecule (e.g., H_2O, methanol) and the MOF backbones to the high polarity-selectivity.

Conclusion

Polycrystalline Pc-based 2D *c*-MOF thin films with large area (cm^2) were synthesized at the liquid-solid interface and displayed high charge transport. Benefiting from the intrinsic electrical conductivity (0.3–0.6 S cm), porous backbone, and abundant $Ni(NH)_4$/Pc units as well as film processability, the resultant 2D *c*-MOF films were taken as active layers and

integrated into chemiresistive sensors for probing water and VOCs detection. Upon further surface-hydrophobic-modification, the surface wettability of the 2D *c*-MOF films could be tailored from hydrophilic to hydrophobic, which resulted in the reduction of diffused H_2O molecules into the sample during the humidity sensing. Thus, a fast recovery progress was successfully achieved at an ultralow humidity level, superior to those of the pristine film samples and the thus-far reported MOFs. Furthermore, the chemiresistors delivered a selective response toward VOCs, due to the strong affinity of the polar analytes to the 2D *c*-MOF backbones. Notably, toward methanol sensing, the devices exhibited an excellent response/recovery (36/13 s) performance at room temperature, which surpassed the currently reported chemiresistors based on the other electroactive materials at room temperature, including MOFs, conducting polymers, metal disulfides and black phosphorus. Our work opens the opportunities to develop surface-modified 2D *c*-MOF films for selective chemiresistive sensing devices with high performance.

Acknowledgements

We thank financial support from ERC Starting Grant (FC2DMOF, No. 852909), ERC Consolidator Grant (T2DCP), Coordination Networks: Building Blocks for Functional Systems (SPP 1928, COORNETs), EU Graphene Flagship (GrapheneCore3, No. 881603), DFG project (CRC 1415, No. 417590517), H2020-MSCA-ITN (ULTIMATE, No. 813036), H2020-FETOPEN (PROGENY, 899205), the German Science Council, Center for Advancing Electronics Dresden (EXC1056), and Dresden Center for Intelligent Materials (DCIM) by the Free State of Saxony and TU Dresden. We acknowledge Elettra Sincrotrone Trieste for providing access to its synchrotron radiation facilities and we thank Luisa Barba for assistance in using beamline XRD1. We appreciate the Dresden Center for Nanoanalysis (DCN) for the use of facility, and Dr. Mao Wang, Dr. Zhongquan Liao, as well as Dr. Tilo Lübken for variable-temperature conductivity, HR-TEM, and NMR measurement, respectively. We thank Dr. Yu Zhang, Dr. Tao Zhang, and Huanhuan Shi for helpful discussions. Open access funding enabled and organized by Projekt DEAL.

Conflict of Interest

The authors declare no conflict of interest.

Keywords: 2D conjugated MOFs · chemiresistive sensors · polarity selectivity · surface modification · volatile organic compounds

[1] a) M. Hmadeh, Z. Lu, Z. Liu, F. Gándara, H. Furukawa, S. Wan, V. Augustyn, R. Chang, L. Liao, F. Zhou, E. Perre, V. Ozolins, K. Suenaga, X. Duan, B. Dunn, Y. Yamamto, O. Terasaki, O. M. Yaghi, *Chem. Mater.* **2012**, *24*, 3511; b) T. Kambe, R. Sakamoto, K. Hoshiko, K. Takada, M. Miyachi, J. H. Ryu, S. Sasaki, J. Kim, K. Nakazato, M. Takata, H. Nishihara, *J. Am. Chem. Soc.* **2013**, *135*, 2462; c) R. Dong, M. Pfeffermann, H. Liang, Z. Zheng, X. Zhu, J. Zhang, X. Feng, *Angew. Chem. Int. Ed.* **2015**, *54*, 12058; *Angew. Chem.* **2015**, *127*, 12226; d) X. Huang, P. Sheng, Z. Tu, F. Zhang, J. Wang, H. Geng, Y. Zou, C.-a. Di, Y. Yi, Y. Sun, W. Xu, D. Zhu, *Nat. Commun.* **2015**, *6*, 7408; e) T. Chen, J.-H. Dou, L. Yang, C. Sun, N. J. Libretto, G. Skorupskii, J. T. Miller, M. Dincă, *J. Am. Chem. Soc.* **2020**, *142*, 12367.

[2] a) J.-H. Dou, M. Q. Arguilla, Y. Luo, J. Li, W. Zhang, L. Sun, J. L. Mancuso, L. Yang, T. Chen, L. R. Parent, G. Skorupskii, N. J. Libretto, C. Sun, M. C. Yang, P. V. Dip, E. J. Brignole, J. T. Miller, J. Kong, C. H. Hendon, J. Sun, M. Dincă, *Nat. Mater.* **2021**, *20*, 222; b) M. Wang, R. Dong, X. Feng, *Chem. Soc. Rev.* **2021**, *50*, 2764.

[3] G. Wu, J. Huang, Y. Zang, J. He, G. Xu, *J. Am. Chem. Soc.* **2017**, *139*, 1360.

[4] H. Arora, R. Dong, T. Venanzi, J. Zscharschuch, H. Schneider, M. Helm, X. Feng, E. Cánovas, A. Erbe, *Adv. Mater.* **2020**, *32*, 1907063.

[5] L. Sun, B. Liao, D. Sheberla, D. Kraemer, J. Zhou, E. A. Stach, D. Zakharov, V. Stavila, A. A. Talin, Y. Ge, M. D. Allendorf, G. Chen, F. Léonard, M. Dincă, *Joule* **2017**, *1*, 168.

[6] R. Dong, Z. Zhang, D. C. Tranca, S. Zhou, M. Wang, P. Adler, Z. Liao, F. Liu, Y. Sun, W. Shi, Z. Zhang, E. Zschech, S. C. B. Mannsfeld, C. Felser, X. Feng, *Nat. Commun.* **2018**, *9*, 2637.

[7] X. Huang, S. Zhang, L. Liu, L. Yu, G. Chen, W. Xu, D. Zhu, *Angew. Chem. Int. Ed.* **2018**, *57*, 146; *Angew. Chem.* **2018**, *130*, 152.

[8] a) J. Park, M. Lee, D. Feng, Z. Huang, A. C. Hinckley, A. Yakovenko, X. Zou, Y. Cui, Z. Bao, *J. Am. Chem. Soc.* **2018**, *140*, 10315; b) M. Wang, H. Shi, P. Zhang, Z. Liao, M. Wang, H. Zhong, F. Schwotzer, A. S. Nia, E. Zschech, S. Zhou, S. Kaskel, R. Dong, X. Feng, *Adv. Funct. Mater.* **2020**, *30*, 2002664; c) J. Liu, Y. Zhou, Z. Xie, Y. Li, Y. Liu, J. Sun, Y. Ma, O. Terasaki, L. Chen, *Angew. Chem. Int. Ed.* **2020**, *59*, 1081; *Angew. Chem.* **2020**, *132*, 1097.

[9] H. Zhong, M. Ghorbani-Asl, K. H. Ly, J. Zhang, J. Ge, M. Wang, Z. Liao, D. Makarov, E. Zschech, E. Brunner, I. M. Weidinger, J. Zhang, A. V. Krasheninnikov, S. Kaskel, R. Dong, X. Feng, *Nat. Commun.* **2020**, *11*, 1409.

[10] Z. Meng, R. M. Stolz, L. Mendecki, K. A. Mirica, *Chem. Rev.* **2019**, *119*, 478.

[11] M. K. Smith, K. E. Jensen, P. A. Pivak, K. A. Mirica, *Chem. Mater.* **2016**, *28*, 5264.

[12] L. S. Xie, G. Skorupskii, M. Dincă, *Chem. Rev.* **2020**, *120*, 8536.

[13] a) M. G. Campbell, S. F. Liu, T. M. Swager, M. Dincă, *J. Am. Chem. Soc.* **2015**, *137*, 13780; b) M. G. Campbell, D. Sheberla, S. F. Liu, T. M. Swager, M. Dincă, *Angew. Chem. Int. Ed.* **2015**, *54*, 4349; *Angew. Chem.* **2015**, *127*, 4423.

[14] a) F. I. Bohrer, A. Sharoni, C. Colesniuc, J. Park, I. K. Schuller, A. C. Kummel, W. C. Trogler, *J. Am. Chem. Soc.* **2007**, *129*, 5640; b) Z. Meng, J. Luo, W. Li, K. A. Mirica, *J. Am. Chem. Soc.* **2020**, *142*, 21656.

[15] Z. Meng, A. Aykanat, K. A. Mirica, *J. Am. Chem. Soc.* **2019**, *141*, 2046.

[16] a) M. Ko, A. Aykanat, M. K. Smith, K. A. Mirica, *Sensors* **2017**, *17*, 2192; b) M. K. Smith, K. A. Mirica, *J. Am. Chem. Soc.* **2017**, *139*, 16759; c) M. S. Yao, J. J. Zheng, A. Q. Wu, G. Xu, S. S. Nagarkar, G. Zhang, M. Tsujimoto, S. Sakaki, S. Horike, K. Otake, S. Kitagawa, *Angew. Chem. Int. Ed.* **2020**, *59*, 172; *Angew. Chem.* **2020**, *132*, 178.

[17] M. D. Allendorf, R. Dong, X. Feng, S. Kaskel, D. Matoga, V. Stavila, *Chem. Rev.* **2020**, *120*, 8581.

[18] V. Rubio-Giménez, N. Almora-Barrios, G. Escorcia-Ariza, M. Galbiati, M. Sessolo, S. Tatay, C. Martí-Gastaldo, *Angew. Chem. Int. Ed.* **2018**, *57*, 15086; *Angew. Chem.* **2018**, *130*, 15306.

[19] a) R. Dong, P. Han, H. Arora, M. Ballabio, M. Karakus, Z. Zhang, C. Shekhar, P. Adler, P. S. Petkov, A. Erbe, S. C. B.

Mannsfeld, C. Felser, T. Heine, M. Bonn, X. Feng, E. Cánovas, *Nat. Mater.* **2018**, *17*, 1027; b) X. Huang, H. Li, Z. Tu, L. Liu, X. Wu, J. Chen, Y. Liang, Y. Zou, Y. Yi, J. Sun, W. Xu, D. Zhu, *J. Am. Chem. Soc.* **2018**, *140*, 15153.
[20] a) M.-S. Yao, X.-J. Lv, Z.-H. Fu, W.-H. Li, W.-H. Deng, G.-D. Wu, G. Xu, *Angew. Chem. Int. Ed.* **2017**, *56*, 16510; *Angew. Chem.* **2017**, *129*, 16737; b) A. Mähringer, A. C. Jakowetz, J. M. Rotter, B. J. Bohn, J. K. Stolarczyk, J. Feldmann, T. Bein, D. D. Medina, *ACS Nano* **2019**, *13*, 6711; c) A.-Q. Wu, W.-Q. Wang, H.-B. Zhan, L.-A. Cao, X.-L. Ye, J.-J. Zheng, P. N. Kumar, K. Chiranjeevulu, W.-H. Deng, G.-E. Wang, M.-S. Yao, G. Xu, *Nano Res.* **2021**, *14*, 438.
[21] R. Dong, T. Zhang, X. Feng, *Chem. Rev.* **2018**, *118*, 6189.
[22] a) L. E. Kreno, K. Leong, O. K. Farha, M. Allendorf, R. P. Van Duyne, J. T. Hupp, *Chem. Rev.* **2012**, *112*, 1105; b) W.-T. Koo, J.-S. Jang, I.-D. Kim, *Chem* **2019**, *5*, 1938.
[23] a) Q. H. Wang, M. C. Hersam, *Nat. Chem.* **2009**, *1*, 206; b) V. Georgakilas, M. Otyepka, A. B. Bourlinos, V. Chandra, N. Kim, K. C. Kemp, P. Hobza, R. Zboril, K. S. Kim, *Chem. Rev.* **2012**, *112*, 6156.
[24] a) A. Weiss, N. Reimer, N. Stock, M. Tiemann, T. Wagner, *Phys. Chem. Chem. Phys.* **2015**, *17*, 21634; b) K.-J. Kim, J. T. Culp, P. R. Ohodnicki, P. C. Cvetic, S. Sanguinito, A. L. Goodman, H. T. Kwon, *ACS Appl. Mater. Interfaces* **2019**, *11*, 33489.
[25] Y. Ito, A. A. Virkar, S. Mannsfeld, J. H. Oh, M. Toney, J. Locklin, Z. Bao, *J. Am. Chem. Soc.* **2009**, *131*, 9396.
[26] A. Chidambaram, K. C. Stylianou, *Inorg. Chem. Front.* **2018**, *5*, 979.
[27] H. Singh, V. K. Tomer, N. Jena, I. Bala, N. Sharma, D. Nepak, A. De Sarkar, K. Kailasam, S. K. Pal, *J. Mater. Chem. A* **2017**, *5*, 21820.
[28] D. Zhang, J. Tong, B. Xia, *Sens. Actuators B* **2014**, *197*, 66.
[29] P.-G. Su, C.-F. Chiou, *Sens. Actuators B* **2014**, *200*, 9.
[30] Q. Kuang, C. Lao, Z. L. Wang, Z. Xie, L. Zheng, *J. Am. Chem. Soc.* **2007**, *129*, 6070.
[31] J. Feng, L. Peng, C. Wu, X. Sun, S. Hu, C. Lin, J. Dai, J. Yang, Y. Xie, *Adv. Mater.* **2012**, *24*, 1969.
[32] B. Hoppe, K. D. J. Hindricks, D. P. Warwas, H. A. Schulze, A. Mohmeyer, T. J. Pinkvos, S. Zailskas, M. R. Krey, C. Belke, S. König, M. Fröba, R. J. Haug, P. Behrens, *CrystEngComm* **2018**, *20*, 6458.
[33] a) L. D. Bharatula, M. B. Erande, I. S. Mulla, C. S. Rout, D. J. Late, *RSC Adv.* **2016**, *6*, 105421; b) C. C. Mayorga-Martinez, Z. Sofer, M. Pumera, *Angew. Chem. Int. Ed.* **2015**, *54*, 14317; *Angew. Chem.* **2015**, *127*, 14525.
[34] M. Mori, Y. Itagaki, J. Iseda, Y. Sadaoka, T. Ueda, H. Mitsuhashi, M. Nakatani, *Sens. Actuators B* **2014**, *202*, 873.
[35] G. S. Aluri, A. Motayed, A. V. Davydov, V. P. Oleshko, K. A. Bertness, N. A. Sanford, R. V. Mulpuri, *Nanotechnology* **2012**, *23*, 175501.
[36] S. P. P. A. Chandrasekaran, can be found under https://people.chem.umass.edu/xray/solvent.html.
[37] G. Williams, D. C. Watts, *Trans. Faraday Soc.* **1970**, *66*, 80.

Manuscript received: March 31, 2021
Revised manuscript received: May 16, 2021
Accepted manuscript online: May 25, 2021
Version of record online: July 12, 2021

